A Stochastic Formulation for the Description of the Crystal Size Distribution in Antisolvent Crystallization Processes

M. Grosso
Dipartimento di Ingegneria Chimica e Materiali, Università degli Studi di Cagliari, Piazza D'Armi, Cagliari I-09123, Italy

O. Galan
Dept. of Chemical Engineering, Louisiana State University, South Stadium Road, Baton Rouge, LA 70803

R. Baratti and J. A. Romagnoli
Dipartimento di Ingegneria Chimica e Materiali, Università degli Studi di Cagliari, Piazza D'Armi, Cagliari I-09123, Italy

DOI 10.1002/aic.12130
Published online December 18, 2009 in Wiley InterScience (www.interscience.wiley.com).

A stochastic approach to describe the crystal size distribution dynamics in antisolvent based crystal growth processes is here introduced. Fluctuations in the process dynamics are taken into account by embedding a deterministic model into a Fokker-Planck equation, which describes the evolution in time of the particle size distribution. The deterministic model used in this application is based on the logistic model, which shows to be adequate to suit the dynamics characteristic of the growth process. Validations against experimental data are presented for the NaCl–water–ethanol antisolvent crystallization system in a bench-scale fed-batch crystallization unit. © 2009 American Institute of Chemical Engineers *AIChE J,* 56: 2077–2087, 2010
Keywords: antisolvent crystallization, stochastic models, Fokker-Planck equation, geometric Brownian motion

Introduction

In crystallization processes, a tight control of the Mean Crystal Size, MCS, and the Crystal Size Distribution, CSD, are commonly required. A great deal of effort for understanding the main factors that affect the MCS and the CSD has been reported in the literature.[1–6] Traditionally, mathematical modeling of particulate systems (e.g., crystallization) is based-on Structured Population Balances (SPB)[7–10] taking into account the effect of formation, growth, and coagulation of the CSD. However, detailed structured population models demand a comprehensive knowledge of the thermodynamic properties of all the components involved in the system under consideration. In addition, SPB modeling might result in dynamic models largely complex, which cannot be easily used, for instance, in model-based process control design or its real-time implementation.

These considerations motivated the development of alternative (e.g., phenomenological) models that should give a reasonable description of the crystallization process, by retaining the core feature of the process, while allowing their use in on-line application.

During the last years, there has been an increasing interest to describe population dynamics using the Fokker-Planck equation (FPE) that can be regarded as the continuous version of Langevin type SDEs.[11] The use of the FPE approach could be found, for example, to describe the growth of

J. A. Romagnoli: On leave from Department of Chemical Engineering at Louisiana State University.
Correspondence concerning this article should be addressed to R. Baratti at baratti@dicm.unica.it.

tumor cells,[12,13] biological populations,[14–16] and of monomer particles.[17] In this approach, the time evolution of each element of the population is regarded as a possible outcome of a random variable driven by a deterministic term (the counterpart of the convective term of the SPBs). Indeed, each element of the population does not behave in the same manner and some dispersion, for example in size, of the population is always observed. This random variable will be thus characterized uniquely by its probability density function (PDF) whose evolution in time can be described in terms of the FPE. Within this context, the FPE could be considered as an alternative ''structured'' way to develop a population balance, taking into account the natural fluctuations present in the population in any biological system, and allowing describing, in a compact form, the population dynamics.

The population balance, PB, and the FPE approaches aim to describe the evolution of a population, but while the first is based on mechanistic (population balance) models the latter is based on phenomenological (deterministic) models coupled with the FPE. Thus, the latter does not aim to describe the underlying physical mechanisms associated with the crystallization process, as it is in our case, but just how the population of the crystal is evolving in time. To describe this evolution, one needs to describe the possible behavior of a single crystal (the FPE will describe the evolution of the population), and this was obtained by inspecting the evolution of the mean value of the CSD, allowing the selection of the appropriate deterministic model.

Another important difference regards the simplicity of the approaches. In the FPE approach, we need only to understand the global behavior of the process without having a deep chemo-physical knowledge, whereas the PB approach will require the formulation and estimation of the corresponding parameters of the particular kinetics mechanism involved in the crystallization process. One may argue then that a drawback, in using a phenomenological model will prevent the portability of FPE approach since the deterministic model parameters are tailored for the system under consideration. However, even the PB approach will require adjusting the parameters for the different kinetics mechanisms incorporated into the model as well as for the solubility model. From a computational point of view the FPE approach offers an advantage over the PB approach because the model obtained is a linear PDE, while in the PB is a set of (generally) nonlinear PDE.

In a previous work (Galan et al., submitted for publication), we exploit the Fokker-Plank approach to predict the mean crystal size and to develop optimal and robust trajectories for antisolvent addition, here the approach will be extended to predict the whole particle size distribution. Consequently, in this work, we propose a FPE approach, for the description of the crystal growth process, in term of the crystal size distribution (CSD), in a bench-scale fed-batch crystallization unit where antisolvent is added to speed-up the crystal formation process. The crystal growth is modeled as a stochastic process, driven by a classic logistic equation, coupled with a geometric Brownian motion. The resulting model is a FPE, describing the evolution, in time, of the CSD. Furthermore, the formulation of a global model to incorporate the effect of antisolvent is discussed and simulations under different antisolvent feeding strategies are provided. The experimental validation of the global model is presented for the previously simulated operational scenarios.

This article is organized as follows. In the next section, we discuss the features of the deterministic model here adopted and introduce its expansion in the probabilistic framework. The estimation problem associated with the CSD in an antisolvent aided crystallization process is carried out. The use of the FPE s to model the growth of the crystal and its numerical integration are discussed. Subsequently, the validation results of the FPE approach for the NaCl–water–ethanol antisolvent crystallization system are presented. The approach for estimating the associated parameters and comparison of the model predictions against experimental data under different antisolvent feeding conditions are provided. Also, in this section, the formulation of a global model to incorporate the effect of antisolvent is discussed and experimental validations, under different antisolvent feeding strategies, are provided. Finally, the concluding remarks and the perspective of further work are given.

Mathematical Model

Logistic FPEs

The development of ''rigorous'' mathematical models describing the dynamics of crystal growth in crystallization processes is typically based-on population balances. The idea of population balances has been widely used in theoretical ecology and extended to the modeling of particulate systems in chemical engineering. The population balances can be either structured or unstructured models.

At the core of the structured population dynamics, the number of crystals in a fed-batch crystallizer is increased by nucleation and decreased by dissolution or breakage. SPB models provide detailed information regarding the CSD in the crystallization unit. However, they demand a great deal of knowledge on the complex thermodynamic associated with the solute and solvent properties to be adequately incorporated in the population balances. Some important contributions in this subject have been reported in the literature.[2,10]

Furthermore, experimental evidence shows that, for example in the case of antisolvent crystallization, the addition of antisolvent do not only change the properties of the solution (e.g. super-saturation), but also lead to changes in the growth habits of the crystals. Thus, surface morphology is connected with growth mechanisms. That is, during the nucleation and growth of crystals, different types of interactions are involved between growth species (molecules or ions) and the growing surface. These interactions include van der Waals forces, ionic and hydrogen bonds. Therefore, the study of the growth kinetics and surface morphology separately may explain only part of the observed crystal growth behavior.[18–21]

Clearly understanding and modeling the complex interactions, during crystallization, at microscopic scale is rather complex. Therefore, in this work, we rather seek to explain the observed macroscopic behavior in a simplified manner. In this context, crystallization can be visualized as a self-organizing and complex process that is subjected to apparently disordered and erratic phenomena such as turbulence at micro-scale mixing and temperature fluctuations. These fluctuations in turn, affect the crystal growth habits and its morphology. Consequently, in our formulation, in an effort

to explain the observed macroscopic behavior of crystal growth in an antisolved aided crystallization, we make use of the FPE approach. The approaches based on the FPE are superior to other approaches based on Langevin equations or Monte Carlo simulations, as the solution of the FPE results in the ensemble of all the possible solutions of a stochastic differential equation.[11]

In our model formulation and following the discussion above, we introduce a simple unstructured population model, where the crystals are classified by their size, L. The growth of each individual crystal is supposed to be independent by the other crystals and is governed by the same deterministic model. To take into account the growth fluctuations and the unknown dynamics not captured by the deterministic term, a random component can be introduced.[22] This random component can be thought as a geometric Brownian motion[23] (GBM), where the intensity of the fluctuations depends linearly by the crystal size. The stochastic model can thus be written as a Langevin equation of the following type:

$$\dot{L} = h(L,t;u)L + L\eta(t), \quad \forall L > 0 \tag{1}$$

In Eq. 1, $h(L,t,u)$ is the expected rate of growth of L (the deterministic model introduced below), L is the size of the single crystal, t is the time, u is an external input (in the present case the antisolvent feed rate), and the function $\eta(t)$ is a random term assumed as Gaussian additive white noise, i.e.,

$$\begin{aligned} &E[\eta(t)] = 0 \\ &E[\eta(t)\eta(t+\tau)] = 2D(u)\delta(\tau) \end{aligned} \tag{2}$$

where $D(u)$ is the additive noise intensity, that may depend on the operating conditions u.

Equation 1 implies that the crystal size L behaves as a random variable, characterized by a certain PDF $p(L,t)$ such that

$$\frac{dN(L,t)}{N} = p(L,t)dL, \quad \int p(L,t)dL = 1$$

where, dN/N is the relative ratio of crystals in the population having a given dimension between L and L + dL. From a practical point of view, the PDF will coincide with the normalized particle size distribution experimentally observed. Obviously, the PDF $p(L,t)$ will depend on the state variables of the system, i.e., the size L and time t.

It should also be noted that, when the GBM assumption holds, the PDF is a log-normal distribution in the limit case of constant h[24,25] for any D value. When h also depends on L, some (minor) distortions from the ideal log-normal case are however expected. This feature is qualitatively observed for many (although not all) crystalline substances[26] and also in the present case as it will be shown later. Thus, Eq. 1 can be further manipulated:

$$\frac{1}{L}\frac{dL}{dt} = \frac{d\ln L}{dt} = h(L,t) + \eta(t) \Rightarrow \frac{dy}{dt} = g(y;t) + \eta(t) \tag{3}$$

and a new random variable $y = f(L) = \ln L$ is introduced. The variable y can be described in terms of its PDF, $\psi(y,t)$, at any instant of time t and should follow the Fokker-Planck equation (FPE):

$$\partial_t\psi + \partial_y[g(y,t)\psi] - D\partial_{yy}\psi = 0 \tag{4}$$

Equation 4 contains two conceptually different terms: the drift term, $\partial_y[g(y,t)\psi]$, takes into account the deterministic contribution on the growth process (roughly speaking, the dynamics of the population average). Conversely, the diffusive term, $D\,\partial_{yy}\psi$, determines the random motion of the variable y related to fluctuations in the particle growth process.[27,28]

Regarding the deterministic part of the model, our purpose is to choose a model as simple as possible, with a parsimonious number of adjustable parameters. To this end, the Logistic equation is possibly the best-known simple sigmoidal asymptotic function used to describe the time dependence of growth processes in an unstructured fashion,[15,29] i.e.,

$$g(y;\theta) = r\,y\left[1 - \left(\frac{y}{K}\right)\right] \tag{5}$$

In Equation 5, y is the exponential of the size of the single crystal, the crystal growth rate r and the equilibrium mean crystal size K are considered constant for each experimental condition and they are supposed to depend only on the antisolvent flow rate. The present growth model can be regarded as the simplest model taking into account mild nonlinearities. In spite of this simplicity, this model provides the main qualitative features of a typical growth process: the growth follows a linear law at low crystal size values and saturates at a higher equilibrium value.

Using the selected growth model, the FPE can be rewritten as:

$$\partial_t\psi + \partial_y\left(r\,y\left(1 - \frac{y}{K}\right)\psi\right) - D\partial_{yy}\psi = 0 \tag{6}$$

along with the boundary conditions:

$$-g(y)\psi + D\partial_y\psi = 0 \quad \text{at } y = 0, \quad \forall t \tag{7}$$

$$\partial_y\psi = 0 \quad \text{as } y \to \infty, \quad \forall t \tag{8}$$

The reflecting boundary condition in Eq. 7 ensures that the elements of the population will never assume negative values, whereas Eq. 8 ensures the decay condition on $\psi(y,t)$ as y goes to infinity, for any time.[13,14]

Finally, the evolution in time of the probability density is described in terms of a linear, partial differential equation depending on the parameters r (linear growth rate), K (equilibrium mean crystal size) and D (diffusivity), that are assumed to depend on the feeding conditions u. Indeed, the antisolvent feed rate is supposed to affect the crystallization kinetics and the parameters appearing in the model can be finally related to these operating conditions, as we will see later when defining a global model structure.

Numerical integration of the FPE

Numerical integration of the Fokker Planck equation is a demanding task due to the following reasons: first, the solution (i.e., the distribution $\psi(y,t)$) must be positive and its

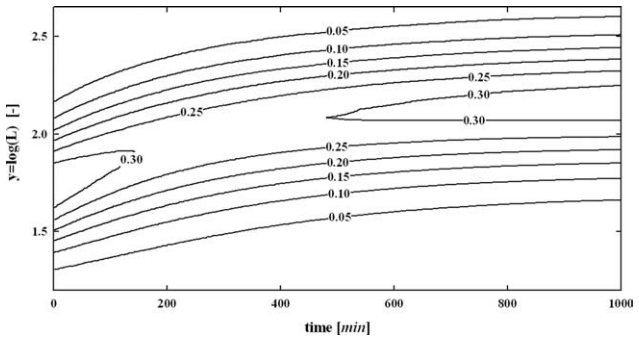

Figure 1. Numerical integration of the model. Iso-level surface of the PDF in the *L-t* plane.

integral over its domain must be unitary; in addition, the domain of the PDF is infinite and this implies that any numerical method has to assume a large enough domain, such that the domain of the PDF can be assumed to be contained in it for all practical purposes. The numerical solution of Eq. 6, with the boundary conditions (Eqs. 7 and 8), is obtained by using orthogonal collocation method on finite elements.[30,31]

In spite of its simplicity the model, Eq 6, shows some interesting features of a stochastic process. One example of possible dynamics of the model is reported in Figures 1 and 2, with parameter values: $K = 5.0$, $r = 5 \times 10^{-3}$ min^{-1}, $D = 5 \times 10^{-4}$ min^{-2}, and with a log-normal distribution with mean $\mu_0 = 4.0$ and standard deviation $\sigma_0 = 0.5$, as initial condition. For sake of clarity, the probability density is hereafter reported in the decimal logarithmic scale although it has been computed in the natural logarithmic one. In more detail, Figure 1 reports the iso-level curves for the distribution function $\psi(y,t)$ in the y-t plane. It appears that the time evolution of the density has not a trivial behavior: the maximum of the distribution function tends to monotonically increase toward its steady state value, according to the deterministic contribution of the Fokker Planck. On the other hand the distribution tends to spread at intermediate values of time, before shrinking back to its steady state condition. This peculiarity is evidenced in Figure 2, where some snapshots of the distribution are reported at different times. It appears that, at intermediate time values, the diffusivity in the model tends to spread the distribution function, then, as time increases the deterministic drift term allows a narrowing of dispersity during growth. This example shows how the competition between diffusive and deterministic drift term can, in principle, allow the description of non trivial behavior.

Parameter Estimation and Model Validation

Experimental data analysis

The NaCl-Water-Ethanol system is used in this study as antisolvent crystallization system. A detailed description of the experimental set-up and the experimental procedures were reported elsewhere.[5,10] Here, suffice to say that, in all experiments, purified water by a Milli-Q system was used. The purities of sodium chloride (NaCl) salt (Merck) and ethanol (Merck) used in the experiments were 99.5% and 99.9%, respectively. Ethanol was added to the aqueous NaCl solution using a calibrated digital dosing pump (Grundfos, Denmark). Temperature was controlled, at 25°C for all experiments, using a Pt100 thermocouple connected to heating/cooling circulator (Lauda, Germany). Infrequent samples were removed iso-kinetically from the crystallizer for particle size and density measurements and in particular the particle size was measured using Mastersizer 2000 particle size analyzer (Malvern Instruments, U.K.).

The same experimental results as reported before[5,10] will be used, where three different antisolvent (ethanol) feeding conditions, at a feed-rates of 0.83, 1.65, and 3.2 mL/min, were performed. Hereafter, we will refer to them as low (LFR), medium (MFR) and high flow-rate (HFR) conditions, respectively. The first acquisition time, labeled as t_0, for each run will be considered as the initial condition used for the FP model calibration, and the second and the final times are labeled, respectively with t_1 and t_f.

Figure 3a shows a typical CSD observed experimentally, in particular, the distribution observed for the MFR condition at $t = 26.5$ min. Nevertheless, this scenario is qualitatively similar for all the experimental observations. It clearly appears that the CSD shows a bimodal shape: at high sizes the distribution of the crystals follows a symmetric bell shaped curve when analyzed in the logarithmic scale, whereas a significant tail is observed at lower sizes. The presence of a low size tail is mainly due to secondary nucleation phenomena which lead to a not negligible ratio of crystals still nucleating even after the principal nucleation has been terminated. On the other hand, the main part of the distribution is close to a normal law. This aspect is more evident (see Figure 3b), when the corresponding cumulative distribution function (CDF) is reported in the normal probability scale (solid line). One should remind that, if the CDF was a normal distribution, this kind of plot would appear as linear, whereas other distribution types will introduce some curvature.

For this case, a deviation from the ideal linear case is observed only in the region of very small crystals, and then it may be concluded that the basic shape of the particle size distribution reminds a Gaussian distribution when analyzed in the logarithmic scale, and thus, it will be similar to a log-normal one when observed in the linear scale. This scenario is compatible with a decaying nucleation rate accompanied by a surface controlled growth,[24,32] and confirms that the GBM assumption is a reasonable choice for the present experimental scenario.

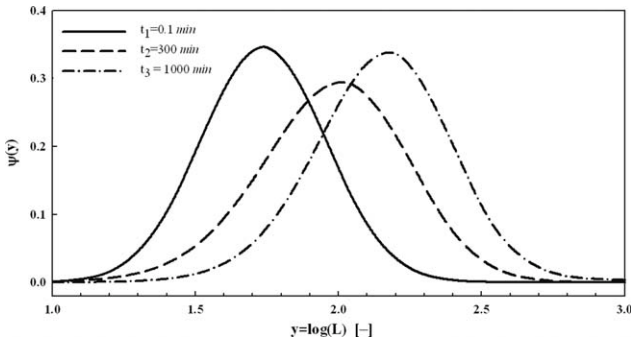

Figure 2. Numerical integration of the model. Snapshots of the probability density function at *t* = 0.1 min (solid line), *t* = 300 min (dashed line), *t* = 1000 min (dashed-dotted line).

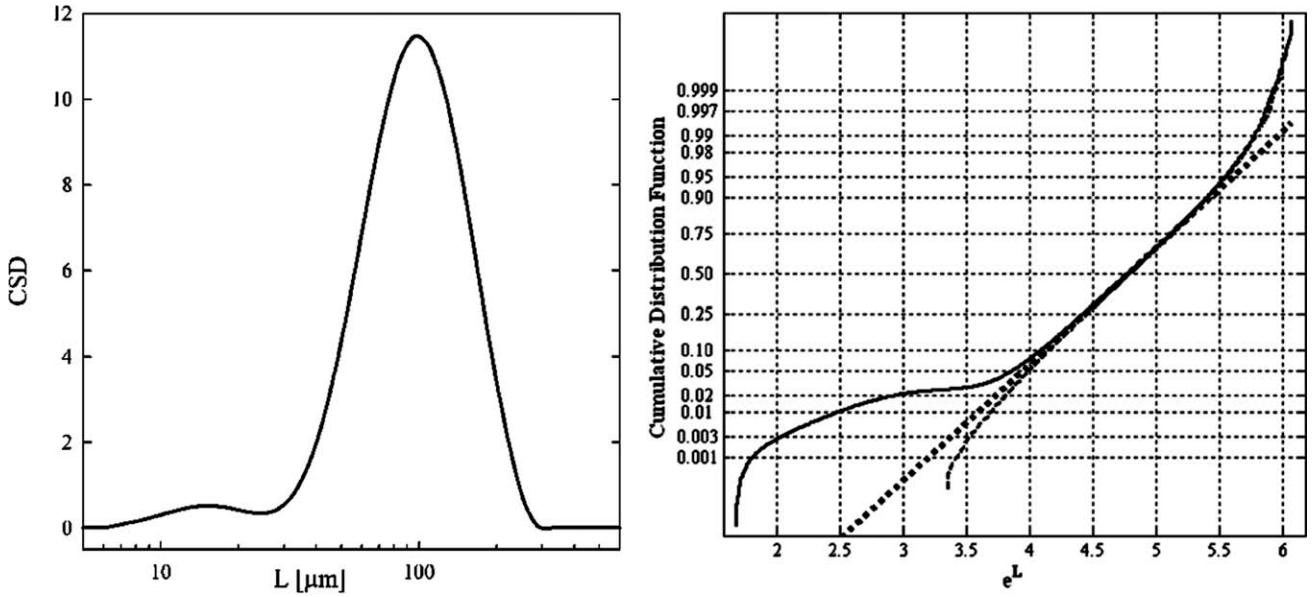

Figure 3. (a) Experimental particle size distribution at time t = 26.5 min (MFR condition); (b) Experimental crystal size (logarithmic scale), the corresponding adjusted Cumulative Distribution obtained by removing the low crystal size tail (dashed line), ideal Gaussian distribution is represented by the dotted line.

The tails at low size values come from secondary nucleation, whose mechanism is not described by the current model, and for this reason, this part of the experimental CSD will be neglected in the current analysis. Therefore, the data will be filtered by removing the points at low size values, with a shape-preserving piecewise cubic interpolation. For sake of completeness, the adjusted Cumulative Distribution obtained by removing the low crystal size tail (dashed line), is also reported in the Figure 3b, where it is possible noticing a qualitative agreement with the Gaussian ideal case.

Parameter estimation/validation

As previously discussed, the parameters, $\boldsymbol{\theta}$ of the model (i.e. the velocity growth rate, r, the saturation value K, and the diffusion, D) are assumed to depend on the antisolvent feeding rate u. As a consequence the model calibration is carried out separately for every run. To reduce the correlation between parameters, nonlinear parameter inference has been accomplished by considering the logarithm of D, thus, the parameters to be estimated are:

$$\boldsymbol{\theta} = \{-\log(D), r, K\} \tag{9}$$

Direct measurements of the particle size distribution are available at n different spatial locations and at m different time values for every operating condition (i.e., antisolvent flow rate). The set of parameters θ is estimated by using the least square criterion, thus searching the minimum of the objective function:

$$V(\theta) = \sum_{i=1}^{m}\sum_{j=1}^{n}[\psi(y_j, t_i; \theta) - \psi^*(y_j, t_i)]^2 \tag{10}$$

In Eq. 10, $\psi(y_j,t_i)$ is the PDF evaluated through numerical integration of Eq. 6, at time t_i and size coordinate y_j, while the distribution $\psi^*(y_j,t_i)$ is the experimental observation of the PSD for the size coordinate y_j at time t_i.

The model calibration is thus carried out by comparing n observation points of the distribution (where $n \sim 40$), monitored at m different times (m between 6 and 10, depending on the experimental run). The number of points used for the parameter inference for each run is thus equal to $m{\cdot}n$. The minimization of the objective function in Eq. 10 is carried out using the Levenberg-Marquardt method.

In our validation approach, a supplementary run at intermediate feeding rate was used for *a-posteriori* model validation. The parameter estimation values together with an estimation of the mean square error are given in Table 1 for the experimental runs. For sake of completeness the m value for every run is also reported.

The mean square error (s^2) is here defined as:

$$S^2 = \frac{\sum_{i=1}^{m}\sum_{j=1}^{n}[\psi(y_j, t_i; \theta) - \psi^*(y_j, t_i)]^2}{(m \cdot n)} \tag{11}$$

Equation 11 provides a Maximum Likelihood estimator for the variance. As the number of experimental points is much larger than the number of parameters ($m{\cdot}n >> 3$), the bias introduced in the estimation is negligible.

Table 1. Point Estimation of the Parameters for the Three Runs

Operating condition	m	$-\log(D)$	$r\times10^2$	K	$S^2\times10^4$
LFR	10	2.402	1.788	4.8779	7.96
MFR	7	2.391	1.800	4.8640	2.84
HFR	6	1.702	8.475	4.6781	4.09

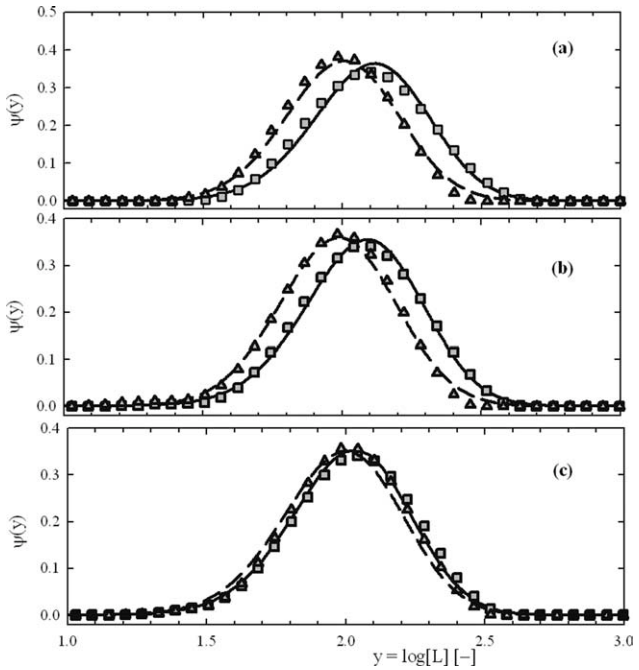

Figure 4. Comparison between model and the experimental Particle size distributions at different times for the three antisolvent feed-rates.

Triangles are the experimental observation at initial time, $t_1 = \{17.2 \text{ min}, 15.5 \text{ min}, 7.0 \text{ min}\}$, dashed lines are the corresponding model predictions; square points are the experimental observations at final time $t_\infty = \{240.0 \text{ min}, 120.0 \text{ min}, 60.0 \text{ min}\}$, solid lines are the corresponding model predictions. Operating conditions: (a) LFR; (b) MFR; (c) HFR. The crystal size is in the decimal logarithmic scale.

The comparison between experiments and model is also carried out by reporting the time evolution of the main moments of the distribution $p(L,t)$, i.e. the mean

$$\mu_L(t) = \int_{0^+}^{\infty} Lp(L,t)dL \tag{12}$$

and the variance

$$\sigma_L^2(t) = \int_{0^+}^{\infty} [L - \mu_L]^2 p(L,t)dL \tag{13}$$

In Figure 4, we report, in decimal logarithmic scale, the first available experimental data at time t_1 and at the end of each run at time t_f (shown respectively with triangles and squares) compared with the computed predictions (dashed line for time $t = t_1$, and solid line at time $t = t_f$). In detail, Figure 4a reports the comparison for the operating condition LFR, Figure 4b reports the comparison for MFR, and Figure 4c reports the results observed for HFR.

The agreement between model and observations is rather remarkable, demonstrating that the proposed model is able to quantitatively capture the shape of the CSD. This is further confirmed by the small values observed for the mean square error s^2 for all the experimental conditions, as reported in Table 1.

Figure 5 shows the first moment experimentally observed (square points) compared with the theoretical predictions (solid line) for the three runs as a function of time. The mean was calculated through Eq. 11. Obviously, there is a coincidence between experiments and model at the first time instant, in view of the choice of the initial condition. The agreement is however rather good at each time and the FPE model, driven by its deterministic part (the logistic growth term), correctly describes the increasing trend of the average crystal growth.

Figure 6 shows the variance $\sigma_L^2(t)$ experimentally observed (square points) compared with the theoretical predictions (solid line) for the three runs, as calculated through Eq. 12. Once more, agreement between model and observations is rather good also for the set of experiments. It is worth stressing out that the variance prediction is rather crucial in crystallization processes as the main focus is on obtaining the least possible dispersion on the crystal size.

In Figure 7, we report the comparison of the model predictions against experimental data provided by a second experimental run under the middle run, not used for the calibration of the model. It can be seen that the model shows remarkable accuracy when validated against experimental data not used for the model calibration.

The parameter inference is further analyzed by exploiting typical tools of the statistical inference. In more detail, the asymptotic correlation matrix for the parameters and the joint confidence regions for the linearized model can be

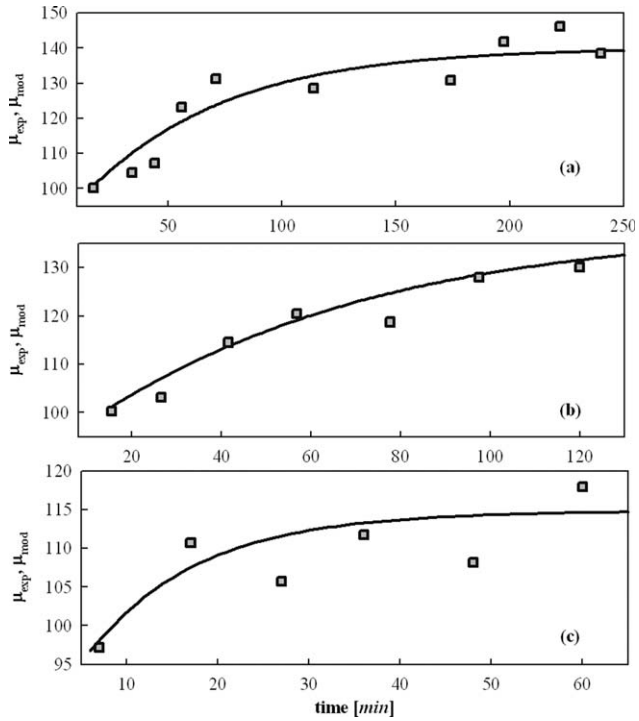

Figure 5. Mean of the Crystal Size Distributions for the three feeding rates Square points are the experimental observation, solid lines are the model predictions.

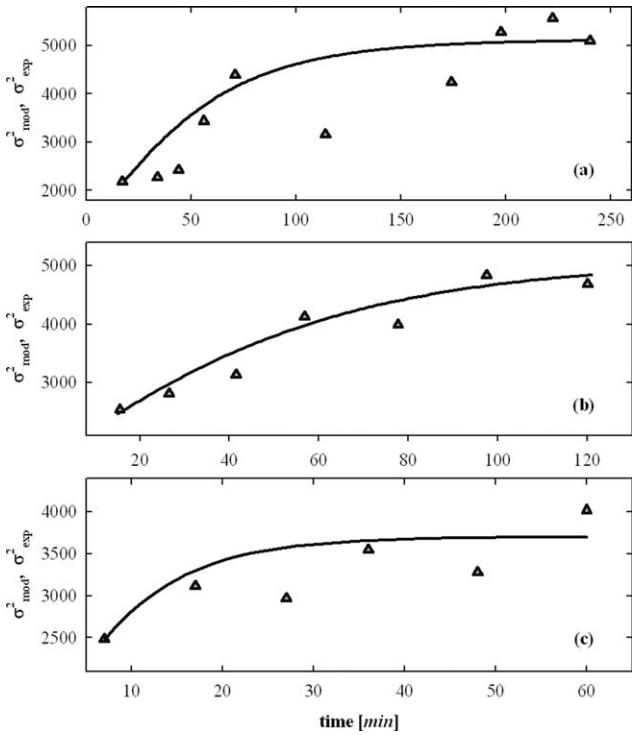

Figure 6. Variance of the Crystal Size Distributions for the three feeding rates Square points are the experimental observation, solid lines are the model predictions.

addressed. Mathematical details for their determination can be found elsewhere (e.g., Refs. 33–35).

Table 2 reports the asymptotic correlation matrix estimated for the first experimental run. For sake of brevity the results of only one run are shown. However, they do not qualitatively change also for the other experimental conditions. A relatively high correlation is observed only between the parameters r and $log(D)$. This is reasonable as these two parameters are both related to the characteristic time of the process, and some dependence between them is then expected. On the other hand, the other parameters are not significantly correlated, thus revealing that ill-conditioning in the parameter inference is prevented, at least for the current experiments.

Table 2. Asymptotic Correlation matrix for the Parameters Estimated for the LFR Experiments

	log(D)	r	K
log(D)	1.0	−0.7663	−0.3281
r		1.0	0.5192
K			1.0

The linear approximations of the joint confidence regions in the parameter space are shown in Figure 8. As we have three parameters to be estimated, the confidence regions will lie in a 3-D parameter space and they will be defined by three different confidence ellipsoids (for the three different runs) as reported in Figure 8a. For sake of clarity also their projections on the different parameter planes are reported in the same Figure 8b–d.

As a first comment, it should be noted that the confidence regions are relatively small, meaning that the parameters are estimated with a small uncertainty. In addition, they do not assume negative values, thus meaning that all of them are statistically significant in the model.

The experiments at low and intermediate feed rates (LFR and MFR) lead to really close values for the parameters, also from a statistical point of view and a partial overlapping of the confidence regions is observed. Roughly speaking, the parameters of the phenomenological model do not change significantly at small and intermediate feeding rates. This aspect could suggest that feeding rate conditions have a minor impact on the growth dynamics at relatively low feed rates. Conversely, at the highest feed run, the estimated parameters are significantly different.

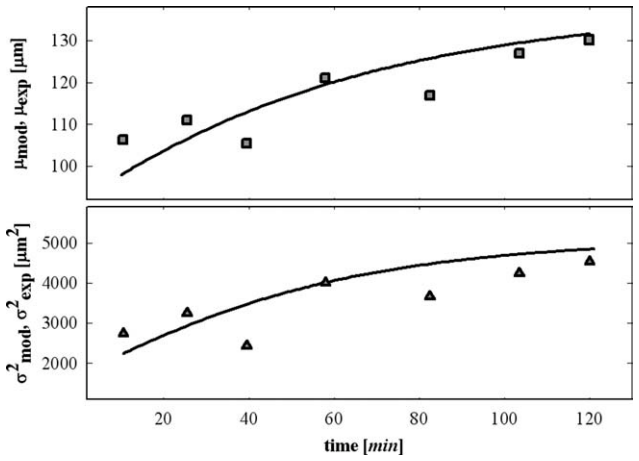

Figure 7. Mean and variance of the Crystal Size Distributions validation against experimental data not used for the parameter inference and here used for a-posteriori validation.

Square points are the mean experimental observation, triangles are experimental variance observations, solid lines are the model predictions.

Global model development

The proposed Fokker-Planck-based model for the crystallization process does not have an explicit dependency of the control input u (i.e. antisolvent flow rate), although this variable does affect the process dynamics. To use the model over the whole operational range a relationship between the parameters θ of the model and the antisolvent flow rate needs to be established.

Consider our model, represented by Eqs. 5 and 6 corresponding to a particular regime, "l" (as defined by the antisolvent flowrate condition). Then, the local model at "l" can be expressed as:

$$g_l(y;\theta_l) = r_l y\left[1 - \left(\frac{y}{K_l}\right)\right] \qquad l = 1.2.3 \qquad (14)$$

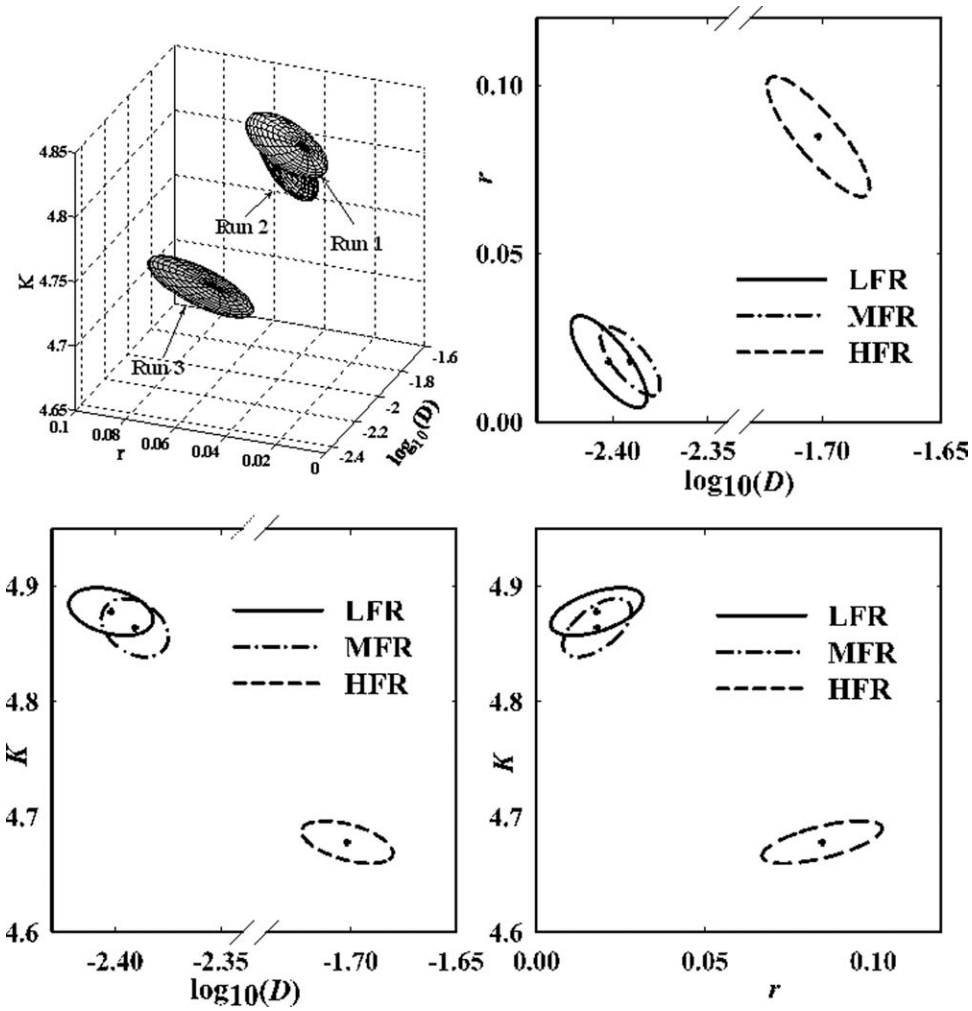

Figure 8. Confidence ellipsoids for the parameter estimations (panel a) and their projections on the three different planes: (b) log(D) vs *r*; (c) log(D) vs *K*; (d) *r* vs *K*. LFR: solid line, MFR: dashed-dotted line; HFR: dashed line.

$$\partial_t \psi_l + \partial_y \left(r_l y \left(1 - \frac{y}{K_l} \right) \psi \right) - D_l \partial_{yy} \psi_l = 0, \qquad l = 1, 2, 3 \tag{15}$$

Here, we have assumed three possible regions corresponding to low, medium and high antisolvent flowrate. This local model structure parameterized by the vector θ is only valid within a particular operating regime and may not be valid in any other operating regime of the system. The local parameters θ_l are obtained through model identification as described earlier. The Figure 9 shows the dependency of the parameters with the antisolvent flow-rate. The observed dependency of the parameters on the antisolvent flowrate could be

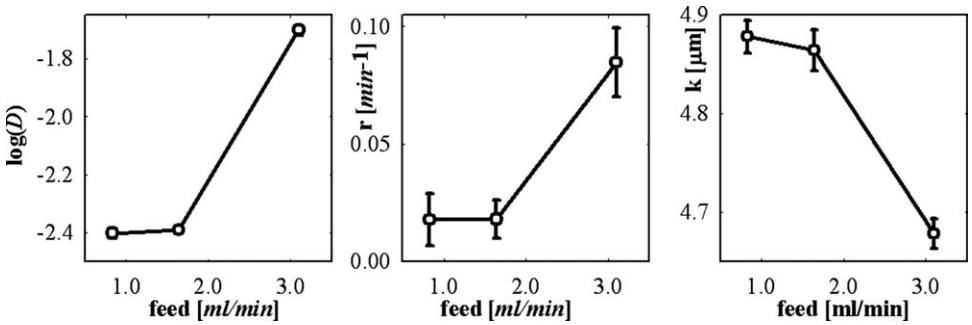

Figure 9. Parameters of the model as a function of the antisolvent flow-rate.

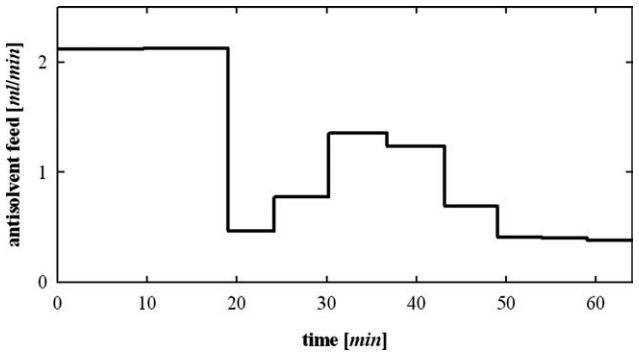

Figure 10. Experimental antisolvent addition policy used for validation.

interpreted as the effect of the super-saturation (crystallization driving force) promoted by the antisolvent. Increasing the antisolvent flowrate (as reported in the literature) will increase the super-saturation (crystallization driving force) that in turn will increase the nucleation effects and the growth of the crystals. The parameters of the phenomenological model will reflect this situation since r and D are increasing and K is decreasing.

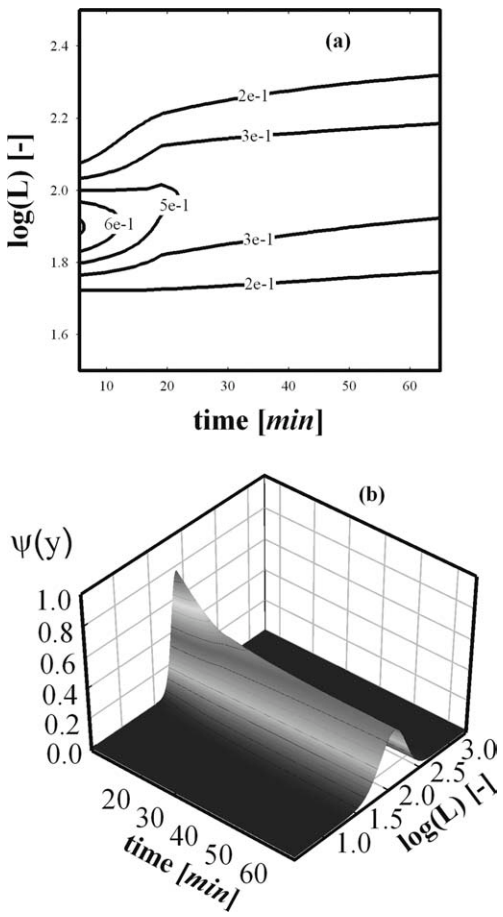

Figure 11. Evolution of the simulated CSD for given antisolvent feeding strategy and corresponding iso-level plot.

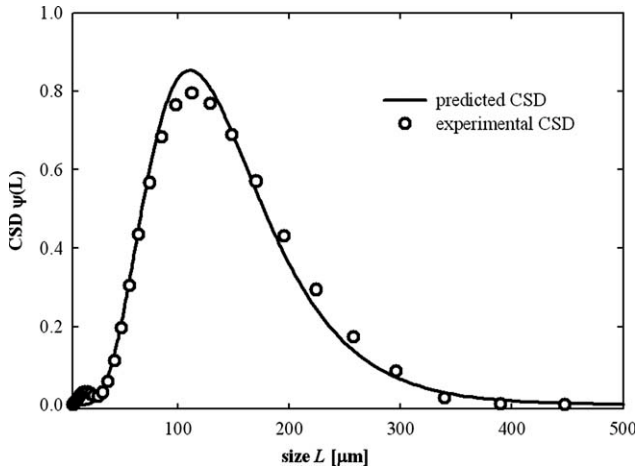

Figure 12. End of the run experimental CSD and the predicted by the global model.

Experimental results (circle) and model (solid lines).

In our formulation the functionality of the model with the antisolvent flowrate is achieved by a piece-wise linear interpolation of the parameters for different antisolvent flow rates. This functionality with the antisolvent flow rate allows the merger of multiple set of parameters for different operating regimes to a single model in the all operating envelop.

Global model validation

This section focuses on the validation of the global model performance to predict the evolution of the mean crystal size when a desired antisolvent addition policy is implemented in the reactor to achieve a given product characteristic.

An optimal antisolvent addition strategy previously proposed in the literature[5] is used to validate the performance of the global model. The proposed strategy targets at obtaining small mean crystal size thus maximizing nucleation. The antisolvent addition policy used for validation of the global model is depicted in Figure 10 and the corresponding simulated evolutions of the CSD is shown in Figure 11.

The antisolvent addition policy starts at a high value of the flow and it is reduced after 20 min with small variations around a small final value. The corresponding crystal growth rate is high and it quickly settles at the desirable low value. The behavior is explained based on the fact that the high concentration of antisolvent in the solution promotes nucleation and the formation of new crystals affecting the size distribution and given a narrow distribution at steady-state conditions.

As in the simulation stage, the antisolvent flow rate policy given in Figure 10 was implemented experimentally for validation. Figure 12 illustrates the comparison between the predicted (using the global model obtained previously) and the experimental values for the final value at the end the run. From this Figure, it is possible noticing that the agreement between the experimental and predicted CSD is rather good, thus indicating that the above approach is a valid alternative to first principle model.

Conclusions

A stochastic phenomenological model for the description of antisolvent mediated crystal growth processes is here introduced. The size of each crystal is supposed to be subjected to a GBM, and its evolution in time is independent from the other crystals in the sample. A deterministic growth term is added to the stochastic model and is expressed as a simple logistic equation. The choice of this simple model is motivated to the parsimonious number of adjustable parameters to take into account. It is further assumed that these model parameters depend on the feed rate conditions. With this approach, the crystal size is a random variable, whose probability density evolution in time can be described in terms of a FPE.

The model is tested on data provided in a bench-scale fed-batch crystallization unit where antisolvent is added to speed-up the crystal formation process. The agreement between experiments and model is quantitative. In detail, a quantitative estimation of the dispersity (i.e. the variance of the PDF) is also appreciated.

A thorough statistical analysis was carried out to quantify the significance and the uncertainty of the estimated parameters, showing that all the parameters affect the physics of the process. This analysis has also given useful insights on the changes in the process dynamics as the operating conditions change.

The FPE formulation appears as a powerful predictive tool, as confirmed by the good agreement also with experiments not used in the model calibration procedure. The approach seems eventually promising to be exploited also for particle size control policies to determine the optimal antisolvent feed rates strategies. It also worth stressing that the proposed approach could be applied also that the cases of crystallization induced by cooling and joint cooling/antisolvent crystallization operations.

Acknowledgments

Jose Romagnoli kindly acknowledges the Regione Sardegna for the support through the program "Visiting Professor 2008". Massimiliano Grosso acknowledges PRIN-2006091953 project for its financial support.

Notation

D = FPE diffusivity, min^{-1}
K = equilibrium mean crystal size
L = crystal size, μm
m = number of experiments
n = number of sampling points for the experimental CSD
p = PDF in the linear scale
r = crystal growth rate, min^{-1}
s = Mean square error
t = time min
t_f = final time min
u = external input
y = crystal size in the logarithmic scale

Greek letters

δ = Dirac delta
η = white noise, min^{-1}
μ = mean of the PDF in the linear scale μm
σ = standard deviation of the PDF in the linear scale μm^2
ψ = probability density function in the logarithmic scale

Literature Cited

1. Xie W, Rohani S, Phoenix A. Dynamic modelling and operation of a seeded batch cooling crystallizer. *Chem Eng Commun*. 2001;187:229–249.
2. Worlitschek J, Mazzotti M. Model-based optimization of particle size distribution in batch-cooling crystallization of paracetamol. *Cryst Growth Des*. 2004;4:891–903.
3. Hu Q, Rohani S, Wang DX, Jutan A. Nonlinear kinetic parameter estimation for batch cooling seeded crystallization. *AIChE J*. 2004;50:1786–1794.
4. Caillet A, Sheibat-Othman N, Fevotte G. Crystallization of monohydrate citric acid 2. Modelling through population balance equations. *Cryst Growth Des*. 2007;7:2088–2095.
5. Nowee SM, Abbas A, Romagnoli JA. Model-based optimal strategies for controlling particle size in anti-solvent crystallization operations. *Cryst Growth Des*. 2008;8:2698–2706.
6. Lindenberg C, Krattli M, Cornel J, Mazzotti M, Brozio J. Design and optimization of a combined cooling/antisolvent process. *Cryst Growth Des*. 2009;9:1124–1136.
7. Ramkrishna D. *Population Balances. Theory and Applications to Particulate Systems in Engineering*. San Diego: Academic Press, 2000.
8. Bakir T, Othman S, Fevotte G, Hammouri H. Nonlinear observer of crystal-size distribution during batch crystallization. *AIChE J*. 2006;52:2188–2197.
9. Qamar S, Elsner MP, Angelov IA, Warnecke G, Seidel-Morgenstern A. A Comparative study of high resolution schemes for solving population balances in crystallization. *Comput Chem Eng*. 2006;30:1119–1131.
10. Nowee SM, Abbas A, Romagnoli JA. Antisolvent crystallization: Model identification, experimental validation and dynamic simulation. *Chem Eng Sci*. 2008;63:5457–5467.
11. Risken H. *The Fokker-Planck Equation: Methods of Solutions and Applications*. Berlin: Springer-Verlag, 1996.
12. Mei DC, Xie CW, Zhang L. The stationary properties and the state transition of the tumor cell growth model. *Eur Phys J B*. 2004;41:107–112.
13. Lo CF. Stochastic Gompertz model of tumor cell growth. *J Theor Biol*. 2007;248:317–321.
14. Soboleva TK, Pleasants AB. Population growth as a nonlinear stochastic process. *Math Comput Modell*. 2003;38:1437–1442.
15. Grosso M, Cella R, Baratti R. Development of a probabilistic model for the plant growth in the nursery phase. In: 3rd International Symposium on Food and Agriculture Products: Processing and Innovations, September 24–26, Naples, (I), 2007:275.
16. Huang DW, Wang HL, Feng JF, Zhu ZW. Modeling algal densities in harmful algal blooms (HAB) with a stochastic dynamics. *Appl Math Modell*. 2008;32:1318–1326.
17. Matsoukas T, Lin Y. Fokker-Planck equation for particle growth by monomer attachment. *Phys Rev E*. 2006;74:031122.
18. Sangwal K. On the mechanism of crystal growth from solutions. *J Cryst Growth*. 1998;192:200–214.
19. Takiyama H, Tezuka N, Matsuoka M, Ristic RI, Sherwood JN. Growth rate enhancement by microcrystals and the quality of resulting potash alum crystals. *J Crystal Growth*. 1998;192:439–447.
20. Kitamura M. Crystallization and transformation mechanism of calcium carbonate polymorphs and the effect of magnesium ion. *J Colloid Interface Sci*. 2001;236:318–327.
21. Roqué J, Molera J, Vendrell-Saz M, Salvado N. Crystal size distributions of induced calcium carbonate crystals in polyaspartic acid and Mytilus edulis acidic organic proteins aqueous solutions. *J Cryst Growth*. 2004;262:543–553.
22. Gelb A. *Applied Optimal Estimation*. Cambridge (Massachusetts): M.I.T. Press, 1988.
23. Mantegna RN, Stanley HE. *An Introduction to Econophysics: Correlation and Complexity in Finance*. Cambridge: Cambridge University Press, 2000.
24. Kile DE, Eberl DD, Hoch AR, Reddy MM. An assessment of calcite crystal growth mechanism based on crystal size distributions. *Geochimica et Cosmochimica Acta*. 2000;64:2937–2950.
25. Dufresne D. The log-normal approximation in financial and other computations. *Adv Appl Prob*. 2004;36:747–773.

26. Eberl DD, Srodon J, Kralik M, Taylor BE. Ostwald ripening of clays and metamorphic minerals. *Science*. 1990;248:474–477.
27. Randolph AD, Larson M. *Theory of Particulate Processes: Analyses and Techniques of Continuous Crystallization*. San Diego: Academic Press, 1988.
28. Olesen P, Ferkinghoff-Borg J, Jensen MH, Mathiesen J. Diffusion, fragmentation, and coagulation processes: analytical and numerical results. *Phys Rev E*. 2005;72:031103.
29. Tsoularis A, Wallace J. Analysis of logistic growth models. *Math Biosci*. 2002;179:21–55.
30. Carey GF, Finlayson BA. Orthogonal collocation on finite elements. *Chem Eng Sci*. 1975;30:587–596.
31. Villadsen J, Michelsen MI. *Solution of Differential Equation Models by Polynomial Approximation*. New Jersey: Prentice Hall, 1978.
32. Eberl DD, Kile DE. Crystal growth rate law identified from changes in variance of crystal size distributions. 15th Annual V M Goldschmidt Conference. *Geochimica Et Cosmochimica Acta*. 2005;69:A402–A402.
33. Seinfeld JH, Chen WH. Estimation of parameters in partial differential equations from noisy experimental data. *Chem Eng Sci*. 1971;26:753–766.
34. Kulkarni K, Zhang LB, Linninger AA. Model and parameter uncertainty in distributed systems. *Ind Eng Chem Res*. 2006;45:7832–7840.
35. Bates DM, Watts D. *Nonlinear Regression Analysis and Its Applications*. New Jersey: Wiley, 2007.

Manuscript received July 23, 2009, and revision received Oct. 28, 2009.